Quantum Electronics **51** (4) 323–332 (2021)

https://doi.org/10.1070/QEL17504

Generation of intense coherent electromagnetic radiation during the interaction of a multi-terawatt laser pulse with a nanowire target*

V.V. Kulagin, V.N. Kornienko, V.A. Cherepenin, D.N. Gupta, H. Suk

Abstract. **Generation of coherent radiation in the IR and terahertz ranges during the propagation of a multi-terawatt laser pulse along a nanowire target is investigated. In the process of interaction, dense electron bunches are displaced from the target and accelerated in the laser field, generating intense electromagnetic radiation. Three regimes of interaction can be realised depending on the duration and shape of the laser pulse. In the first regime, when the laser pulse is long enough (tens and hundreds of femtoseconds), electrons are only partially forced out of the target. The characteristics of the low-frequency part of the spectrum of the generated radiation are determined in this case by the duration of the laser pulse, as well as by its amplitude and target parameters (geometric dimensions and concentration of electrons). In the second regime, the laser pulse has a large amplitude and a steep rising edge (the amplitude of the first half-wave is of the order of the maximum pulse amplitude); as a result, most of the electrons are displaced from the target already at the initial moment of interaction. In this regime, unipolar and bipolar pulses with a duration of tens of laser field periods can be formed. Changing the target length makes it possible to control the period of field oscillations and their number in the generated radiation. In the intermediate regime of short laser pulses with an insufficiently steep rising edge, oscillations of the formed electron bunches can occur in the macroscopic Coulomb attraction field of the charged target, which gives rise to radiation with a frequency several times lower than that of laser radiation. In this case, the pulses of the generated radiation contain a few cycles of the field with decreasing amplitude and increasing frequency. Using numerical simulation in three regimes of interaction, the characteristics of IR and terahertz radiation are found, in particular, the pulse shapes, ranges of generated frequencies, amplitudes and angular distributions of radiation are determined. It is shown that the amplitude of the generated pulse can reach subrelativistic and relativistic values (the field strength is more than 1 TV m^{-1} at a frequency ten times lower than the laser radiation frequency), and the energy conversion efficiency can be of the order of one percent.**

Keywords: *interaction of high-power laser pulses with matter, acceleration of electrons by laser pulses, generation of terahertz and IR radiation, nanoscale targets.*

1. Introduction

The development of methods for generating terahertz and IR radiation is of great importance for many fields of science and technology [1–3], including visualisation of the internal structure of objects, remote electromagnetic sensing, biomedical diagnostics, study of material characteristics, terahertz spectroscopy, including nonlinear one, acceleration of electrons and ions, etc. For the formation of terahertz and IR fields with a high intensity, the most promising is the use of plasma as a working medium, since in this case, there are no limitations associated with breakdown, while high-power laser pulses are an excellent option for exciting plasma. Terahertz radiation was first experimentally recorded in the study of the propagation of a laser pulse in a plasma in 1993 [4]. Since then, a large number of different schemes have been proposed and studied [5–21] based on solid-state and gas targets: a high-power laser pulse ionises them and then interact with the resulting plasma.

At present, nanofilms have become one of the traditional types of solid targets widely used in laser-plasma experiments. The thickness of nanofilms can be several nanometres, and the transverse dimensions significantly exceed the diameter of the laser beam and reach hundreds of micrometres. If a non-adiabatic laser pulse with sufficient power is normally incident on such a target, then all electrons are synchronously displaced from the nanofilm and accelerated under the action of the longitudinal (along the laser beam axis) component of the Lorentz force [22, 23]. The first experiments convincingly demonstrated the formation of relativistic electron bunches during the interaction of high-power laser pulses with nanofilms [24–26].

The generation of coherent terahertz and IR relativistic pulses at normal incidence of a high-power non-adiabatic laser pulse on a nanofilm strip of limited width was studied in [13, 16, 19]. During the interaction of a laser pulse with a solid target, dense electron bunches are displaced from the target and accelerated in the laser field, generating intense electromagnetic radiation due to acceleration. The concentration of electrons in the formed bunches and their total charge increase

*Reported at the 4th International Conference on Ultrafast Optical Science (Russia, Moscow, FIAN, 28 September – 2 October 2020).

V.V. Kulagin Sternberg Astronomical Institute, Lomonosov Moscow State University, Universitetskii prosp. 13, 119991 Moscow, Russia; Kotel'nikov Institute of Radioengineering and Electronics, Russian Academy of Sciences, ul. Mokhovaya 11, 125009 Moscow, Russia; e-mail: victorvkulagin@yandex.ru;
V.N. Kornienko, V.A. Cherepenin Kotel'nikov Institute of Radioengineering and Electronics, Russian Academy of Sciences, ul. Mokhovaya 11, 125009 Moscow, Russia;
D.N. Gupta Department of Physics and Astrophysics, University of Delhi, Delhi-110007, India;
H. Suk Department of Physics and Photon Science, Gwangju Institute of Science and Technology, 123 Cheomdangwagi-ro, Buk-gu, Gwangju, 61005, South Korea; e-mail: hysuk@gist.ac.kr

Received 14 December 2020; revision received 15 February 2021
Kvantovaya Elektronika **51** (4) 323–332 (2021)
Translated by V.L. Derbov

with an increase in the plasma frequency of the target, which leads to an increase in the maximum radiation amplitude. Therefore, subrelativistic intensities of terahertz and IR radiation can be obtained only with the use of solid targets.

To increase the efficiency of generation of terahertz and IR radiation by the displaced electron bunches the transverse size of the nanofilm should be comparable to the diameter of the laser beam or be smaller than it [19]. This condition can be met not only for nanofilm strips of limited width, but also when using low-dimensional targets, in particular, filamentous targets (nanorods, nanotubes, nanowires).

In this work, we investigated the generation of coherent terahertz and IR radiation generated in the course of propagation of relativistic laser pulses along a filamentary target, which has a length comparable to or greater than the laser radiation wavelength λ in this direction and dimensions significantly smaller than λ in the transverse direction. Similar to the case of normal incidence of a laser pulse on a nanofilm, the physical mechanism of generating radiation with a frequency lower than that of the laser pulse (IR and terahertz ranges) can be associated with partial or complete forcing of electron bunches out of a filamentary target followed by their longitudinal acceleration by the laser pulse field. When the laser field reaches a sufficiently large amplitude, the electrons overcome the Coulomb barrier of the target and begin to accelerate in a direction perpendicular to the axis of the laser beam, emitting a dipole radiation wave. Upon proceeding to the relativistic regime, the longitudinal momentum becomes larger than the transverse one, and the entire electron bunch moves in the direction of propagation of the laser pulse, too [27]; as a result, the bunch trajectory deviates from the perpendicular direction towards the axis of the laser beam. The vector of the total momentum and the directional pattern of the radiation from the bunch also change direction, and the relativistic Doppler effect breaks the symmetry of the dipole radiation pattern, which leads to an increase in the radiation intensity of the bunch in the direction of motion. This process is repeated in each half-period of the laser pulse, resulting in the formation of an inhomogeneous wave. The acceleration time of electron bunches depends on the parameters of the laser radiation and the target and can be much longer than the cycle of the laser field. The emission of a single electron accelerated by a high-power laser pulse is considered, e.g., in [28, 29], and the emission of dense electron bunches from nanoscale targets under the action of a short relativistic laser pulse and their further acceleration by the laser field are studied in [30, 31]. The generation of terahertz radiation using a wire target in the case of weakly relativistic laser pulses was studied in [32, 33].

The efficiency of interaction with filamentous targets can be much higher than with thin films in the regime of normal incidence of a laser pulse, since with an increase in the film thickness (or the electron concentration in it), the reflection coefficient of the laser pulse increases. This reduces the transmission of radiation through the film and, therefore, the strength of the laser field and the time of its interaction with plasma electrons decrease. For a filamentous target, the displaced electrons and the laser pulse copropagate for some time, which increases the duration of their interaction, whilst the field amplitude varies slightly.

Numerical simulations have shown that, depending on the duration and shape of the laser pulse, three regimes of interaction can be realised. In the first regime, when the laser pulse is long enough (from tens to hundreds of femtoseconds), electrons are only partially forced out from the target, and in the optimal case, the process of forcing out occurs during the entire action of the laser pulse. A unipolar pulse propagates from the target in each direction; the low-frequency component of its spectrum can, in a certain approximation, be considered as a result of optical field rectification during its interaction with the target (below, for convenience, we will call this case the optical field rectification regime). The characteristics of the low-frequency part of the spectrum depend on the duration of the laser pulse and its amplitude, as well as on the parameters of the target (geometrical dimensions and concentration of electrons).

In the second regime, the non-adiabatic laser pulse has a large amplitude and a steep rising edge (the amplitude of the first half-wave is of the order of the maximum pulse amplitude). As a result, most of the electrons are displaced from the target already at the initial instant of interaction, and the total duration of the laser pulse does not play a significant role (the non-adiabatic laser pulse regime). Due to the large number of electrons in the displaced bunch, unipolar and bipolar radiation pulses with a duration of tens of laser field periods and a relativistic amplitude can be formed in this regime. Finally, in the intermediate regime of short laser pulses with an insufficiently steep rising edge, some formed bunches of electrons return to the target, and can oscillate in the Coulomb attraction field of ions, which leads to generating radiation with a frequency several times lower than that of laser radiation. In this case, the radiation pulses contain several cycles of the field oscillation with decreasing amplitude and increasing frequency. Since such radiation arises during the Coulomb relaxation of a system perturbed by a laser pulse to a state of equilibrium, below we will call it Coulomb relaxation radiation. The characteristics of IR and terahertz radiation in three regimes of interaction are found, in particular, the characteristic pulse shapes, ranges of generated frequencies, amplitudes and angular distributions of radiation are determined.

2. Interaction of a high-power laser pulse with a filamentous target in the regime of optical field rectification

The generation of electromagnetic radiation during the propagation of a multi-terawatt laser pulse along a filamentary target was investigated by two-dimensional (2D3V) numerical simulation using the fully relativistic XOOPIC code [34]. A Gaussian laser pulse (Fig. 1a) with a wavelength of λ = 1 μm was polarised linearly along the y axis, had a duration of 10 periods of laser radiation (hereinafter, the total duration at the level e^{-1} from the maximum of the field amplitude is indicated) and propagated from left to right along the x axis (the beam axis passes through the centre of the target with the coordinate $y = 55\lambda$). The field distribution in the transverse direction was Gaussian with a beam diameter of 20λ (at the 1/e level for the field strength), and its dimensionless amplitude $a_0 = 10$ (intensity 1.4×10^{20} W cm^{-2}). Hereinafter, the dimensionless field amplitude is determined in accordance with the expression $a_0 = eE_0/(mc\omega)$, where E_0 is the dimensional amplitude of the laser pulse; ω is the laser radiation frequency corresponding to the wavelength λ; e and m are the absolute value of the charge and the rest mass of electron; and c is the speed of light in vacuum. For convenience of comparison, a similar normalisation is applied to the generated field, in particular, to the component B_z. The left edge of the

target was located at a point with coordinates $x = 40\lambda$, $y = 55\lambda$, the target width (size along the y axis) was 0.02λ (20 nm), the length was 0.5λ (size along the x axis), and the initial electron concentration $n = 100n_{cr}$, where $n_{cr} = (m\omega^2)/(4\pi e^2)$ is the critical concentration. In the simulation, it was assumed that the target becomes ionised at the moment of the laser pulse arrival (since $a_0 \gg 1$), and the plasma is cold and collisionless. The mass of ions m_i in the simulation was taken equal to $1840m$. Along the x and y axes, the cell had a size of $1.15 \times 10^{-2}\lambda$, and each cell contained 2000 particles. The size of the simulation window in Fig. 1 was $80\lambda \times 110\lambda$, and in other cases it was $60\lambda \times 60\lambda$. Moving window technology was used in the numerical simulation.

A typical form of the field component B_z during the propagation of a high-power laser pulse along a filamentary solid-state target is shown for two time moments in Fig. 1. After interaction, a spherical wave (cylindrical in 2D simulations) diverges from the target, its parameters (amplitude, duration, and shape of the pulse) changing along its front, and some of the target electrons are carried away by the laser pulse. The amplitude of the laser pulse near the axis slightly decreases due to energy losses for the acceleration of the target electrons and reflection from the target. The shape of the pulses propagating along the y axis (up and down) is shown in Fig. 2. These pulses are slightly different because they correspond to different half-cycles of the laser field (positive and negative); they are unipolar pulses, the duration of which is determined by the duration of the laser pulse. There is also a high-frequency component in the radiation pulses at the frequency of the laser field, since it is polarised in this case along the y axis. For polarisation of the laser field along the z axis, the emitted pulses will be similar (except for the reverse polarity), with the frequency of the high-frequency component being 2ω. Since, as a result of the interaction of laser radiation with the target, a unipolar pulse propagates in each direction, we can say that the optical field is rectified. This statement will be supported below by qualitative considerations. For other values of the system parameters, radiation pulses can also contain short peaks of opposite polarity (see, for example, the right-hand pulse in Figs 2a and 2b, where a short single peak of positive polarity is visible), i.e., be bipolar. The presence of peaks of opposite polarity is associated with the return of part of the accelerated electron bunches to the target before the end of the laser pulse.

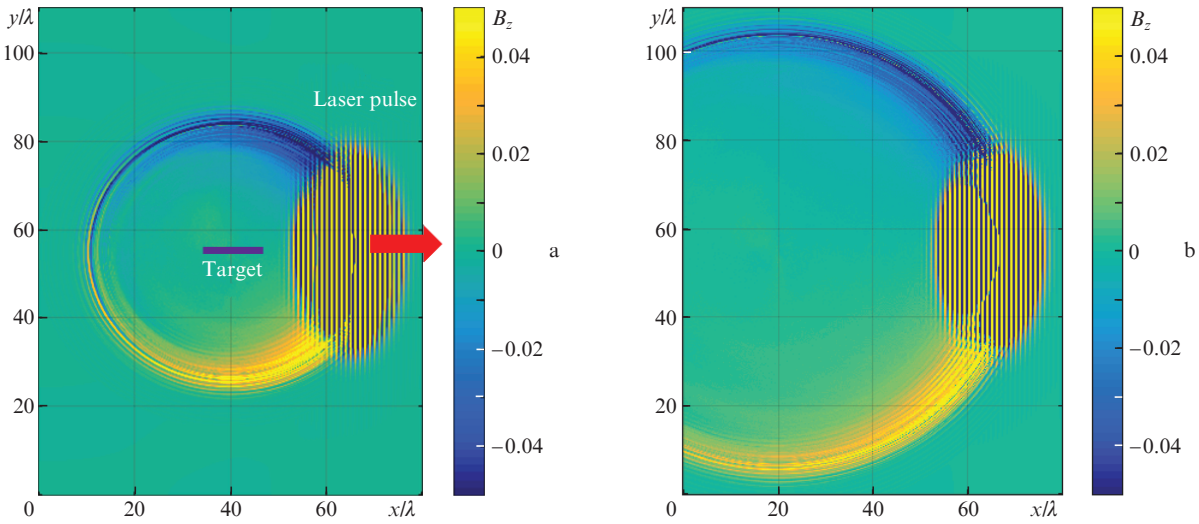

Figure 1. (Colour online) Interaction of a high-power Gaussian laser pulse with a filamentary solid-state target (the image contrast is enhanced for better visibility of the generated field): spatial distributions of the dimensionless component B_z of the field after (a) 40 and (b) 60 periods of laser radiation after the onset of interaction.

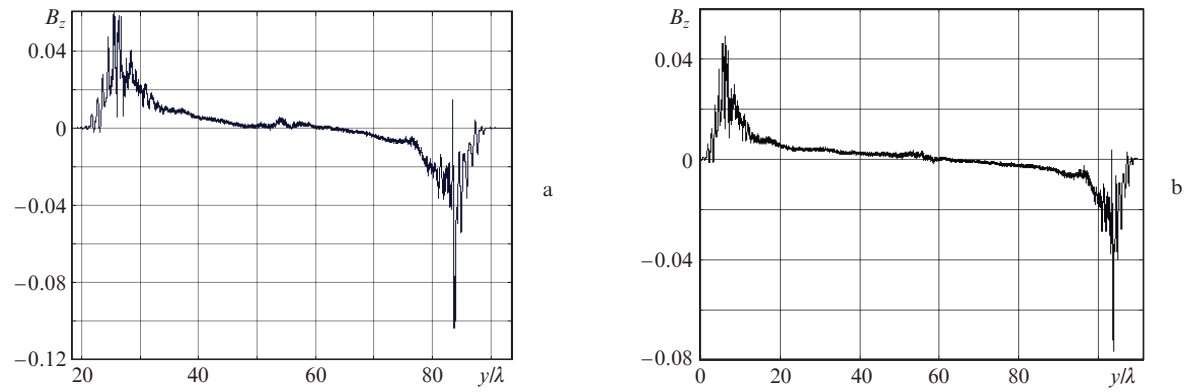

Figure 2. Field component B_z along a straight line passing through the middle of the target parallel to the y axis, (a) 40 and (b) 60 periods after the onset of the interaction. The target is located at a point $y = 55\lambda$.

The shapes of pulses propagating at angles of 90° (right-hand pulse in Figs 2a and 2b) and 45° to the x axis are shown in Fig. 3. The pulses are similar in shape, but their amplitudes differ by a factor of 2.5 (the pulse propagating at an angle of 45° has a larger amplitude). The total pulse lengths are comparable: 12λ for 90° and 14λ for 45°. The low-frequency parts of the spectra $\tilde{B}_z$ of these pulses are shown in Fig. 4. The spectra also have similar characteristics: the spectral width at the 1/e level is 22 THz for 45° and 25 THz for 90°. In both cases, the maximum spectral amplitudes are achieved for the low-frequency components. The parameters of the pulses change along the front of the generated wave (depend on the angle with respect to the direction of the laser pulse propagation) due to the relativistic motion and the change in the velocity direction of the electron bunches forming them upon acceleration by the laser field after escaping from the target, as well as the relativistic transformation of the angular characteristics of the radiation of the bunches.

The initial moment of the laser pulse interaction with the target is shown in Fig. 5. Figure 5a (after 10 periods of the laser field from the onset of the interaction) shows several bunches of electrons emitted from the target. Each bunch is formed by its own half-period of the laser pulse; therefore, bunches expelled in the positive (negative) direction of the y axis follow with a period equal to the period of the field. Radiation in the positive (negative) direction of the y axis is formed by both groups of bunches, while the contribution of bunches emitted in the same direction is the largest (due to the relativistic Doppler transformation of the radiation amplitude). The distributions along the x axis of the transverse (p_y) and longitudinal (p_x) momenta of emitted electrons after 20 periods of the laser field from the onset of the interaction are shown in Figs 5b and 5c. Comparison of these figures shows that the longitudinal momentum p_x is approximately proportional to the square of the transverse momentum p_y. This can be qualitatively explained as follows. After escaping from the target, each bunch falls into the field of an almost plane laser wave, because the displacement of the bunches along the y axis is significantly less than the diameter of the laser beam. For a single electron in a plane wave field, the longitudinal momentum p_x is proportional to the square of the transverse momentum p_y [27]. The transverse momentum of the electron is completely determined by the vector potential of the wave; as a result, the longitudinal momentum p_x of the electron turns out to be proportional to the square of the laser pulse field and exceeds p_y at $a_0 \gg 1$, while the rate of change in p_x is also much greater than the rate of change in p_y. Then, when an electron is accelerated by a wave, the radiation field generated by it along the y axis is determined mainly by the longitudinal pulse p_x, i.e., it is also proportional to the square of

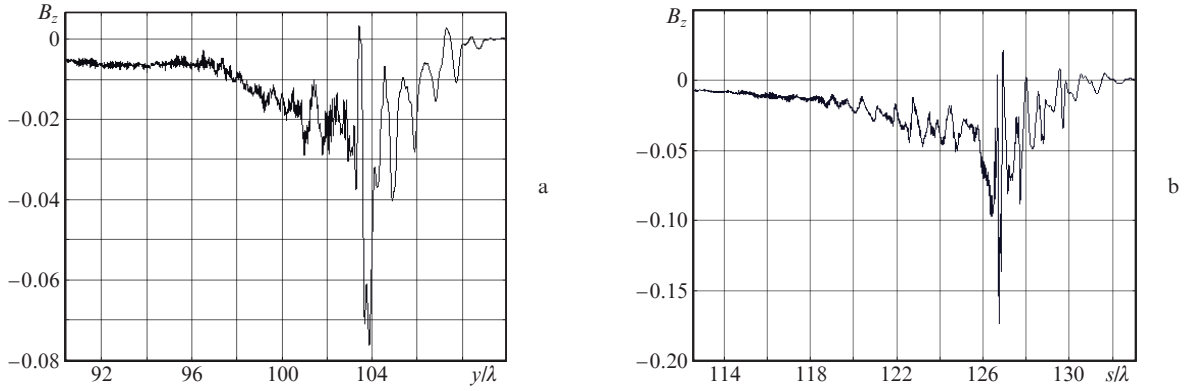

Figure 3. Pulse shapes (component B_z) for angles (a) 90° and (b) 45° relative to the direction of propagation of the laser pulse (after 60 periods from the onset of the interaction; s is the coordinate along a straight line passing through the centre of the target at a certain positive angle to the x axis, measured from the lower end of the straight line).

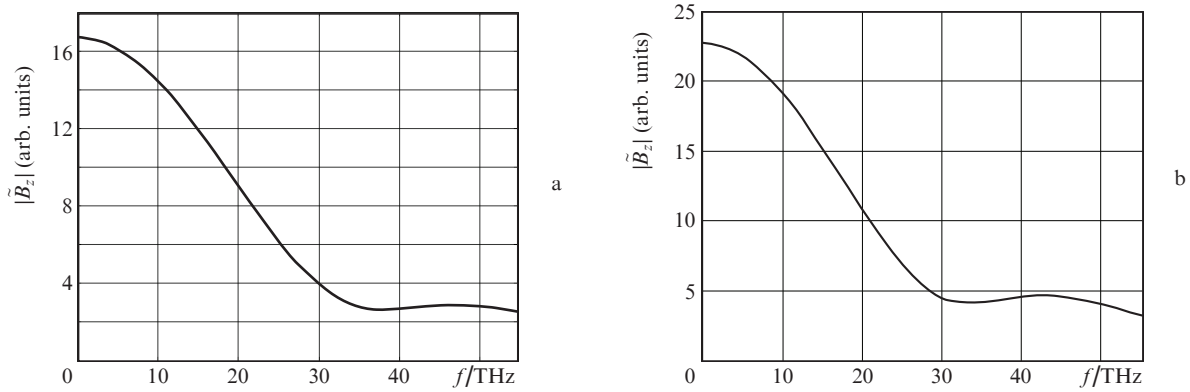

Figure 4. Spectra $|\tilde{B}_z(f)|$ of the pulses for angles (a) 90° and (b) 45° relative to the direction of propagation of the laser pulse (f is the spectral frequency).

the laser pulse field. Thus, the interaction as a whole can be approximately characterised as a rectification of the optical field. This effect, which manifests itself most clearly when analysing the motion of a single electron in the field of a plane wave, in the presence of a target is complicated by the presence of other electrons and the Coulomb force of attraction of ions (see Figs 3a, 5b, and 5c).

The characteristics of the low-frequency part of the generated radiation in this regime depend on the charges of the electron bunches, which are determined by the duration and amplitude of the laser pulse, as well as the concentration of electrons in the target and its geometric dimensions. As the amplitude of the laser pulse increases, the amplitude of the generated pulse also increases, but its duration decreases. This is due to the earlier formation of outgoing bunches, because they begin to form at a certain amplitude of the laser pulse half-wave, and in the case of a Gaussian pulse, several weaker half-waves will always pass before the arrival of the forming half-wave. When the target is depleted (all electrons leave it), the radiation is significantly attenuated; as a result, the duration of the formed pulse decreases. Thus, in this regime, it is important to match the amplitude of the laser pulse with the concentration of electrons in the target in order to obtain a radiation pulse with the longest duration and greatest amplitude.

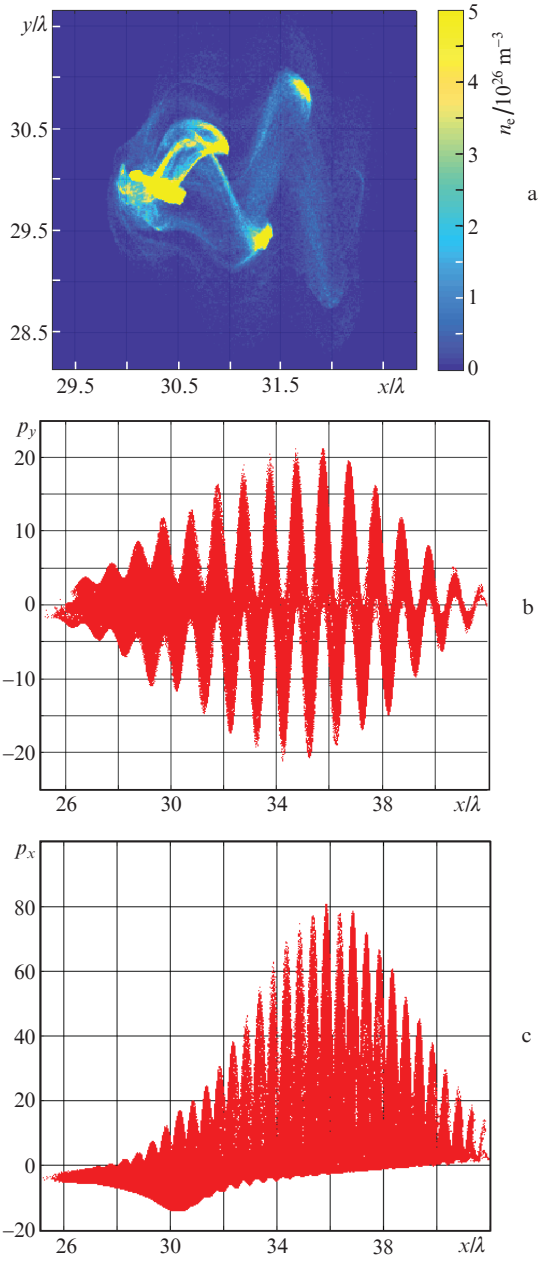

Figure 5. (Colour online) Electron concentration n_e after 10 periods of the laser field from the onset of the interaction (the image contrast is magnified) (a), as well as the distributions of the transverse momentum p_y of electrons along the x axis (b) and the longitudinal momentum p_x along the same axis (c) after 20 periods of the laser field from the onset of the interaction (momenta are normalised to mc).

3. Radiation arising from Coulomb relaxation oscillations of an electron bunch after exciting the target by a short laser pulse

Another mechanism of generation of radiation, whose frequency is low as compared to the frequency of the laser field, is shown in Fig. 6. A Gaussian pulse has a total duration of two periods of laser radiation, its amplitude is $a_0 = 20$, and the target length is 2λ, the other parameters are the same as for Fig. 1. The left edge of the target is located at a point with coordinates $x = 30\lambda$, $y = 30\lambda$. The spatial distribution of the component B_z and the field along a straight line passing through the middle of the target parallel to the y axis are shown in Fig. 6a (on the right side, a laser pulse is seen that passed through the target) and Fig. 6b, respectively.

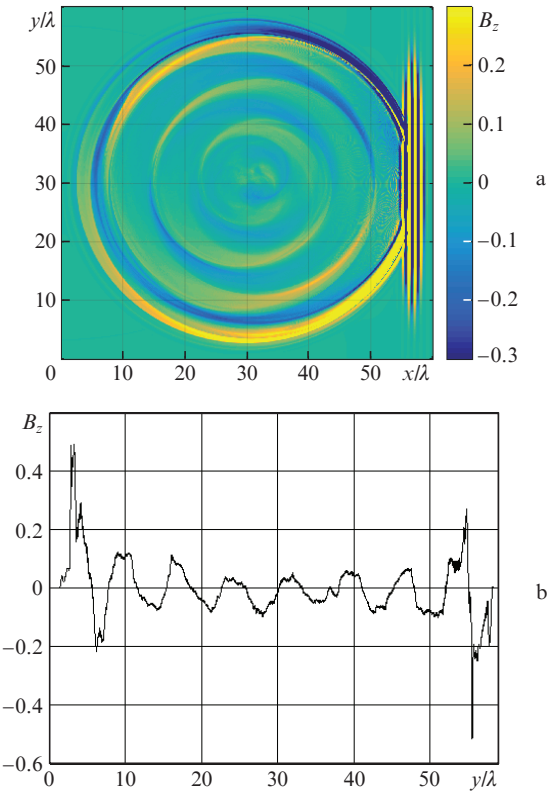

Figure 6. (Colour online) Spatial distribution of the B_z component (a) and the field along a straight line passing through the middle of the target parallel to the y axis (b), 30 periods of the laser field after the onset of the interaction (the image contrast is enhanced).

In this intermediate regime of short laser pulses with an insufficiently steep rising edge, the electron bunches that escaped from the target at the initial stage of interaction, after some time lag behind the laser pulse and are accelerated in the negative direction of the x axis by the macroscopic Coulomb field of the charged target, determined by spatial distributions of ions and returned low-energy electrons. When approaching the target, bunches of electrons can gain relativistic energy; as a result, they fly through the region where the ions are located and begin to oscillate around it along the x axis. The shape and size of the electron bunch continuously change in the course of motion, the maximum size during the first period of oscillations is up to 0.5 μm along the y axis and up to 1.5 μm along the x axis, while the maximum deviations of the bunch centre from the target centre are not greater than 0.3 μm along the y axis and 1.1 μm along the x axis. It should be noted that a bunch can cross the horizontal axis several times in one oscillation period. With such oscillations, the velocity of the bunch along the horizontal axis approaches the speed of light at certain times, which leads to the characteristic radiation pattern shown in Fig. 6. If two or more electron bunches are involved in the oscillations, the radiation pattern can be much more complicated.

The first period of high-amplitude radiation in the positive and negative directions of the y axis is associated with the initial displacement of electron bunches from the target and return to it, while the remaining half-periods are associated with oscillations of the bunches in the Coulomb field of the target. The initial amplitude of the field generated during the oscillation of electron bunches turns out to be of the order of 0.1, then the amplitude decreases, and the period of the oscillations also slightly decreases. The total duration of the radiation pulse is determined by the decay time of the electron bunch. It should be noted that a similar mechanism for generating low-frequency radiation can be realised with nanofilm targets [13].

The shapes of pulses propagating at different angles to the x axis are shown in Fig. 7. A decrease in the duration and an increase in the amplitude of negative half-waves at an angle of 45° and positive half-waves at an angle of 135° is associated with the relativistic Doppler effect [27]. Thus, the half-wave at values of s/λ from 60 to 65 in Fig. 7c (angle 135°) is generated during the relativistic motion of the bunch to the right (in the positive direction of the x axis), and the half-wave at s/λ from 58 to 60 is generated during the bunch motion to the left (in the negative direction of the x axis). At angles close to 90° relative to the x axis, the relativistic Doppler transformation does not play a significant role; therefore, the durations of negative and positive half-waves of radiation field are close (Fig. 7b). Thus, in general, the radiated field has a strong phase modulation and a wide frequency spectrum (Fig. 8), i.e., the radiation is very different from the harmonic one, which is especially pronounced for angles of 45° and 135°. The maximum of the emission spectrum for all angles falls on about 43 THz for the selected simulation parameters and the wavelength turns out to be on the order of seven laser radiation wavelengths. In the emission spectrum, the ratio of the intensities of the second and first harmonics is greatest for an angle of 135°. The maximum amplitude of the Coulomb relaxation radiation is also the largest in this direction, and the durations of the positive half-waves are the smallest. This is because the first return of electron bunches after excitation to the initial position of the target occurs when moving in the negative direction of the x axis, since the laser pulse moves to the right. At the first return, the bunches are still relatively dense and compact, and the amplitude of their oscillations is greatest, then the size of the bunches grows, and the concentration of electrons in them decreases, the amplitude of the oscillations also decreases, and the radiation amplitude decreases. The lowest harmonic level and pulse amplitude are recorded at an angle of 90°. It should be noted that, taking into account the value of the period, the maximum amplitude of the relaxation radiation turns out to be subrelativistic in this case.

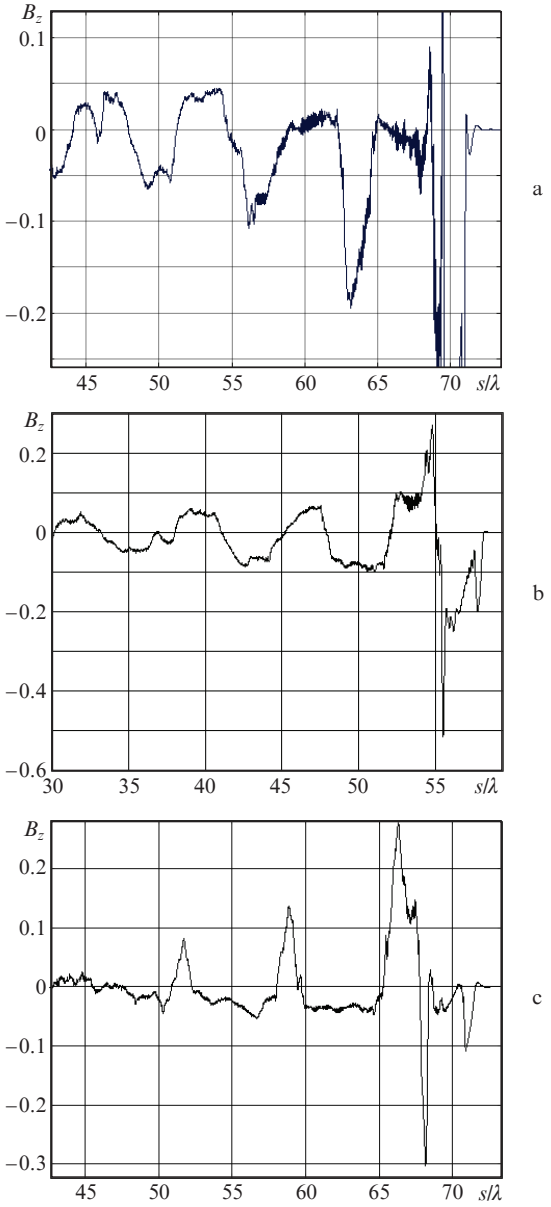

Figure 7. Shapes of pulses propagating at angles of (a) 45°, (b) 90° and (c) 135° to the x axis.

4. Interaction of a high-power non-adiabatic laser pulse with a filamentous target

In this regime, a non-adiabatic laser pulse has a large amplitude and a steep rising edge; as a result, most of the electrons

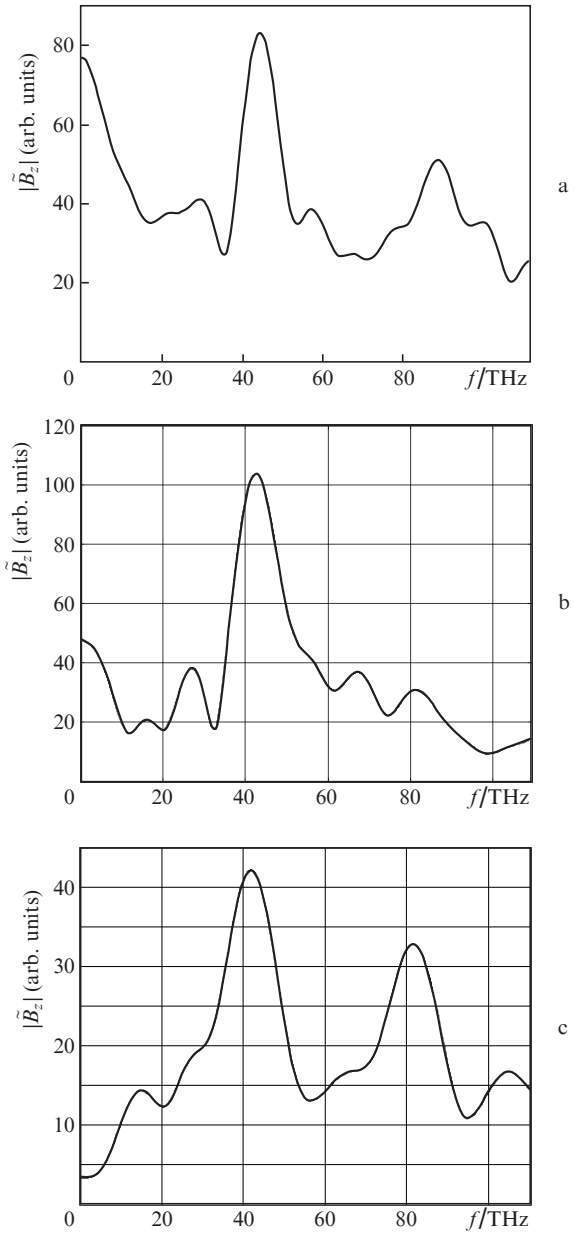

Figure 8. Spectra $|\tilde{B}_z(f)|$ of the pulses propagating at angles of (a) 45°, (b) 90° and (c) 135° to the x axis.

are displaced from the target already at the initial moment of interaction and carried away by the laser pulse. The spatial distribution of the B_z component 20 cycles of the laser field after the onset of interaction is shown in Fig. 9a, and the field along a straight line passing through the middle of the target parallel to the y axis is shown in Fig. 9b. A Gaussian laser pulse has a steep rising edge with an amplitude of the first half-cycle of the field of the order of the maximum pulse amplitude (the rise time is much shorter than the pulse decay duration); the total duration is three cycles of laser radiation. The field is polarised along the z axis, the dimensionless amplitude is 20, and the other parameters are the same as for Fig. 1. The left edge of the target is located at a point with coordinates $x = 30\lambda$, $y = 30\lambda$; its length is 0.5λ. At these parameters, a unipolar pulse with an amplitude of ~0.2 and a total length of $\sim 5\lambda$ is formed, which is similar to bipolar

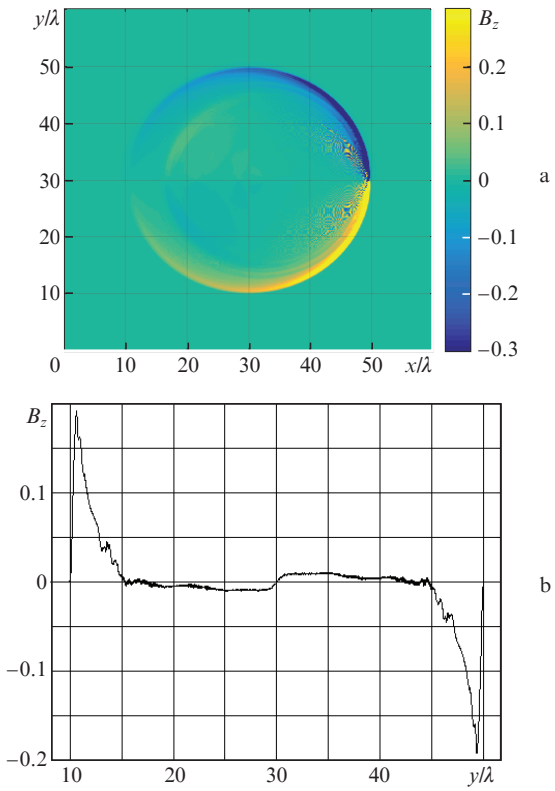

Figure 9. (Colour online) Spatial distribution of the component B_z (a) and the field along a straight line passing through the middle of the target parallel to the y axis (b), 20 periods of the laser field after the onset of interaction.

pulses formed at normal incidence of a nonadiabatic laser pulse on a nanofilm strip of limited width [19].

Figure 10 shows the distribution of the electron concentration 20 cycles of the laser field after the onset of the interaction. On the right, a dense bunch of emitted electrons is visible, which continues to move to the right along with the laser pulse. On the left, a somewhat less dense bunch is also visible, which is formed by electrons that have turned back due to the Coulomb attraction by ions. The target ions are located near a point with $x = 30\lambda$, where the electron concentration is low. The maximum concentration of electrons in a bunch accom-

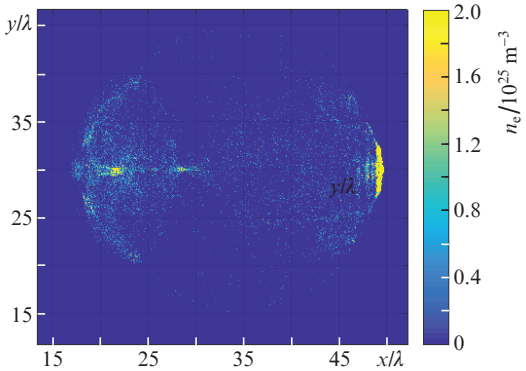

Figure 10. (Colour online) Electron concentration n_e after 20 periods of the laser field from the onset of the interaction, corresponding to Fig. 9a (the image contrast is enhanced).

panying a laser pulse turns out to be almost two orders of magnitude higher than the concentration in other bunches at this time and amounts to about 2×10^{21} cm^{-3}, i.e., the laser pulse carries away most of the target electrons.

An increase in the target length generally leads to the appearance of two radiation sources located near the ends of the target. The spatial distribution of the B_z component after 20 periods of the laser field after the onset of interaction for this case is shown in Fig. 11 (the laser pulse is visible on the right). The target length is 5λ, the laser pulse has a total duration of two cycles of laser radiation, and the other parameters are the same as for Fig. 1. The radiation field is formed as a result of the superposition of two cylindrical waves with axes shifted by the target length and usually has a complex structure. With an even greater increase in the target length and at a fixed laser pulse amplitude, the field structure is qualitatively retained. However, the number of accelerated bunches increases, some of them slow down and turn back, which leads to chaotic generation of short pulses with reverse polarity. As a result, the radiation field in each direction takes the form of a random sequence of short radiation pulses. The possibility of effective use of such fields requires a separate study.

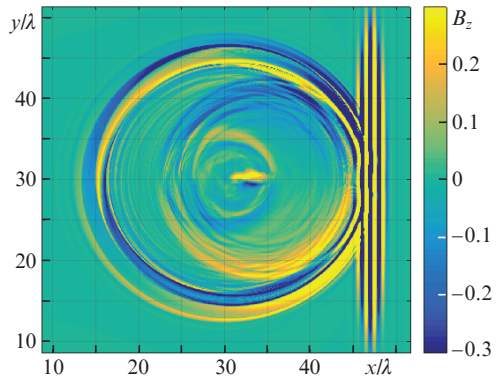

Figure 11. (Colour online) Spatial distribution of the B_z component 20 periods of the laser field after the onset of the interaction (the image contrast is enhanced).

At the same time, by a consistent choice of the target length and the laser pulse amplitude, it is possible to synchronise the radiation pulses from the left and right ends of the target. In this case, the pulses are added coherently, which leads to an increase in both the maximum radiation amplitude and its duration. The spatial distribution of the B_z component for such a case is shown in Fig. 12a, and the field along a straight line passing through the middle of the target parallel to the y axis is shown in Fig. 12b. The target length is 2λ, the other parameters are the same as for Fig. 9. In this case, the maximum radiation amplitude more than doubled and attained 0.45 (the field strength in dimensional units is $\sim$1.5 TV m^{-1} at a distance of 20 μm from the target), the period is approximately 5λ, the pulse becomes bipolar and contains two oscillation cycles. With such parameters, this is already a pulse of relativistic radiation, and its effective dimensionless amplitude, calculated taking into account the real radiation frequency, is 2.25, i.e., the conversion coefficient for the effective dimensionless amplitude turns out to be more than 11% (2.25/20). The value of the dimensionless amplitude plays an important role in the action of radiation pulses on charged particles. The coefficient of conversion of the laser pulse energy into the energy of the generated radiation (the energy efficiency of the process) is, in this case, $\sim$0.7%. The energy of the laser pulse used in the simulation is 8.6 J (the required peak power of the laser pulse is $\sim$850 TW); therefore, the energy of the generated radiation reaches 60 mJ. A further matched increase in the laser pulse amplitude and target length leads to an increase in the radiation amplitude and period. For example, by increasing the laser pulse amplitude to 50 and the target length to 5λ, one can obtain radiation pulses with an amplitude of 0.7 and a period of 10λ, while the pulse shape approximately corresponds to Fig. 12b. Here, the conversion coefficient for the effective dimensionless amplitude reaches 14%, and the conversion coefficient for energy turns out to be $\sim$0.4%. Further increase in the amplitude of terahertz and IR radiation is possible by using the focusing of generated pulses [19]. In addition, since the radiation pulses are formed by the rising edge of the laser pulse, its length can be reduced in comparison with that used in the simulation (3λ). The diameter of the laser beam can also be reduced to four to five wavelengths, which will lead to a further increase in the energy efficiency of generation.

Analysis of Figs 9 and 12 shows that an increase in the target length with a constant laser pulse amplitude converts a unipolar pulse into a bipolar one; in addition, the number of

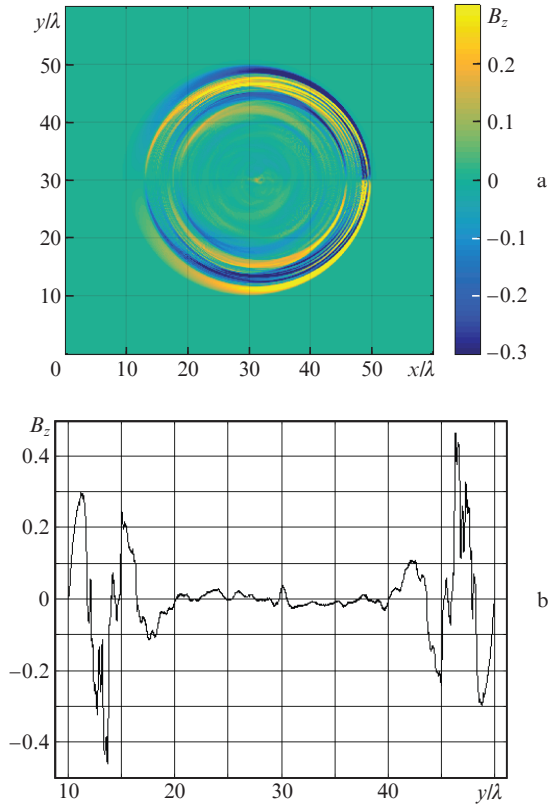

Figure 12. (Colour online) Spatial distribution of the component B_z (a) and the field along a straight line passing through the middle of the target parallel to the y axis (b), 20 periods of the laser field after the onset of interaction.

cycles of the generated radiation increases. This is because low-frequency radiation is formed mainly at the ends of the targets; therefore, the left and right ends emit with a time delay required for the laser pulse to travel the length of the target, resulting in repeated radiation pulses. Unfortunately, the reserves for using this approach when increasing the target length are limited, because the required amplitudes of the laser pulse quickly become too large, for example, for a target with a length of 10λ, $a_0 = 100$ is required (the radiation frequency is 15 THz, and the period is 20λ).

Thus, due to the large number of electrons in the displaced bunch, the interaction of a high-power non-adiabatic laser pulse with a filamentary target can form unipolar and bipolar radiation pulses with a duration of tens of laser periods and a relativistic amplitude. In this case, the radiation characteristics are determined mainly by the amplitude of the half-wave, displacing most of the electrons, and weakly depend on the total duration of the laser pulse. In addition, changing the target length makes it possible to control the value of the period and the number of oscillations of the generated radiation.

5. Discussion of results and conclusions

The longitudinal scheme of interaction of high-power laser pulses with a filamentous target is characterised by a significant increase in the interaction time of electron bunches displaced from the target and the laser pulse compared to the case of its normal incidence on a nanofilm target. The experimental implementation of the considered scheme requires solving the problem of fixing the target in the appropriate way. Indeed, the target is located on the axis of the laser beam; therefore, the presence of any elements supporting it can significantly change the nature of the interaction. However, it should be taken into account that in two-dimensional modelling, the target is assumed to be infinite along the z axis. Consequently, in the experiment, nanofilm strips with a width equal to the length of the filamentous target in two-dimensional simulation can be used. In this case, the strip of the nanofilm should be located along the z axis, and the incidence of the laser pulse should be grazing. The obtained simulation results can be used in experiments if the laser beam has an elliptical cross section with the length of the major axis much larger than the nanofilm width (size along the x axis), or for a conventional laser beam with a circular cross section with the diameter much larger than the nanofilm width.

Thus, in this paper, we investigated the generation of coherent radiation in the IR and terahertz ranges during the propagation of a multi-terawatt laser pulse along a nanowire target. In the process of interaction, dense electron bunches are displaced from the target and accelerated in the laser field, generating intense electromagnetic radiation. It is shown that, depending on the duration and shape of the laser pulse, three regimes of interaction can be realised.

In the first regime – the regime of the optical field rectification – the laser pulse can be quite long (tens and hundreds of femtoseconds), and electrons are only partially forced out of the target. In this case, the generated radiation has the form of unipolar pulses, and the characteristics of the low-frequency part of their spectrum are determined by the duration of the laser pulse, as well as by its amplitude and target parameters. In the second regime, the non-adiabatic laser pulse has a large amplitude and a rather steep rising edge (the amplitude of the first half-wave is of the order of the maximum pulse amplitude). As a result, most of the electrons are displaced from the target immediately at the initial stage of interaction. In this regime, relativistic unipolar and bipolar pulses with a duration of tens of laser field periods can be formed. Changing the length of the target allows controlling the value of the period and the number of periods in the generated pulse. Finally, in the intermediate regime of short laser pulses with an insufficiently steep rising edge, relaxation oscillations of the formed electron bunches can arise in the macroscopic Coulomb field of a charged target after its excitation, which gives rise to Coulomb relaxation radiation with a frequency several times lower than that of laser radiation. In this case, the pulses of the generated radiation contain several cycles of field oscillation with decreasing amplitude and increasing frequency.

Using numerical simulation, the characteristics of IR and terahertz radiation are found in three regimes of interaction, in particular, the pulse shapes, ranges of generated frequencies, amplitudes and angular distributions of radiation are determined. It is shown that the amplitude of the generated pulse can reach subrelativistic and relativistic values (the field strength in dimensional units is $\sim$1.5 TV m^{-1} at a distance of 20 μm from the target), and the energy conversion efficiency can be about 0.5%–0.7%. More detailed studies of radiation in three regimes will be presented in subsequent publications.

Acknowledgements. The work was supported by the Russian Foundation for Basic Research and Department of Science and Technology of the Government of India (Scientific Project No. 19-52-45035-Ind-a). D.N. Gupta is grateful to the Department of Science and Technology of the Government of India for financial support (Joint Project DST-RFBR 2020 No. INT/RUS/RFBR/394). H. Suk thanks the National Research Foundation of Korea for the support (Project NRF2017R1A2B3010765).

References

1. Ferguson B., Zhang X.C. *Nat. Mater*., **1**, 26 (2002).
2. Williams G.P. *Rep. Prog. Phys*., **69**, 301 (2006).
3. Reimann K. *Rep. Prog. Phys*., **70**, 1597 (2007).
4. Hamster H., Sullivan A., Gordon S., et al. *Phys. Rev. Lett*., **71**, 2725 (1993).
5. Carr G.L., Martin M.C., McKinney W.R., et al. *Nature*, **420**, 153 (2002).
6. Sheng Z.-M., Mima K., Zhang J., Sanuki H. *Phys. Rev. Lett*., **94**, 095003 (2005).
7. Wu H.-C., Sheng Z.-M., Zhang J. *Phys. Rev. E*, **77**, 046405 (2008).
8. Jahangiri F., Hashida M., Nagashima T., et al. *Appl. Phys. Lett*., **99**, 261503 (2011).
9. Wu H.-C., Meyer-ter-Vehn J., Ruhl H., Sheng Z.-M. *Phys. Rev. E*, **83**, 036407 (2011).
10. Li Y.T., Li C., Zhou M.L., et al. *Appl. Phys. Lett*., **100**, 254101 (2012).
11. Gopal A., Herzer S., Schmidt A., et al. *Phys. Rev. Lett*., **111**, 074802 (2013).
12. Uryupin S.A., Frolov A.A. *Quantum Electron*., **43**, 1132 (2013) [*Kvantovaya Elektron*., **43**, 1132 (2013)].
13. Kulagin V.V., Kornienko V.N., Cherepenin V.A. *Uchen. Zap. Fiz. Fak-ta Mosk. Un-ta*, (4), 144337 (2014).
14. Kuratov A.S., Brantov A.V., Aliev Yu.M., Bychenkov V.Yu. *Quantum Electron*., **46**, 1023 (2016) [*Kvantovaya Elektron*., **46**, 1023 (2016)].
15. Gupta D.N., Kulagin V.V., Suk H. *Opt. Commun*., **401**, 71 (2017).
16. Kulagin V.V., Kornienko V.N., Cherepenin V.A., Gupta D.N. *Zh. Radioelektron*., (1) (2017); http://jre.cplire.ru/jre/jan17/15/text.pdf.

17. Kuratov A.S., Brantov A.V., Aliev Yu.M., Bychenkov V.Yu. *Quantum Electron*., **48**, 653 (2018) [*Kvantovaya Elektron*., **48**, 653 (2018)].
18. Brantov A.V., Kuratov A.S., Maksimchuk A., Aliev Yu.M., Bychenkov V.Yu. *EPJ Web Conf*., **195**, 03002 (2018).
19. Kulagin V.V., Kornienko V.N., Cherepenin V.A., Gupta D.N., Suk H. *Quantum Electron*., **49**, 788 (2019) [*Kvantovaya Elektron*., **49**, 788 (2019)].
20. Hu K., Yi L. *Phys. Rev. A*, **102**, 023530 (2020).
21. Chand G.M., Gopal K., Gupta D.N., Kulagin V.V., Suk H. *IEEE Trans. Plasma Sci*., **48**, 3727 (2020).
22. Kulagin V.V., Cherepenin V.A., Hur M.S., Suk H. *Phys. Rev. Lett*., **99**, 124801 (2007).
23. Kulagin V.V., Cherepenin V.A., Gulyaev Y.V., et al. *Phys. Rev. E*, **80**, 016404 (2009).
24. Kiefer D., Henig A., Jung D., et al. *Eur. Phys. J. D*, **55**, 427 (2009).
25. Paz A., Kuschel S., Rodel C., et al. *New J. Phys.*, **14**, 093018 (2012).
26. Kiefer D., Yeung M., Dzelzainis T., et al. *Nat. Commun*., **4**, 1763 (2013).
27. Landau L.D., Lifshits E.M. *The Classical Theory of Fields: Volume 2* (Course of Theoretical Physics Series) (London: Butterworth-Heinemann, 1980; Moscow: Nauka, 1988)].
28. Hartemann V., Troha A.L., Luhmann N.C., Toffano Z. *Phys. Rev. E*, **54**, 2956 (1996).
29. Hartemann V. *Phys. Plasmas*, **5**, 2038 (1998).
30. Bulanov S.S., Maksimchuk A., Krushelnick K., et al. *Phys. Lett. A*, **374**, 476 (2010).
31. Di Lucchio L., Gibbon P. *Phys. Rev. Spec. Top. Accel. Beams*, **18**, 023402 (2015).
32. Zhuo H.B., Zhang S.J., Li X.H., et al. *Phys. Rev. E*, **95**, 013201 (2017).
33. Tian Y., Liu J., Bai Y., et al. *Nat. Photonics*, **11**, 242 (2017).
34. Verboncoeur J.P., Langdon A.B., Gladd N.T. *Comput. Phys. Commun*., **87**, 199 (1995).